† ELECTRONIC SUPPLEMENTARY INFORMATION

3D electrohydrodynamic printing and characterisation of highly conductive gold nanowalls

Patrik Rohner,[a] Alain Reiser,[b] Freddy T. Rabouw,[c,d] Alla S. Sologubenko,[b] David J. Norris,[c] Ralph Spolenak,[b] and Dimos Poulikakos[a]

[a.] Laboratory of Thermodynamics in Emerging Technologies, Department of Mechanical and Process Engineering, ETH Zurich, 8092 Zurich, Switzerland.
[b.] Laboratory for Nanometallurgy, Department of Materials, ETH Zurich, 8093 Zurich, Switzerland.
[c.] Optical Materials Engineering Laboratory, Department of Mechanical and Process Engineering, ETH Zurich, 8092 Zurich, Switzerland.
[d.] Debye Institute for Nanomaterials Science, Utrecht University, Princetonplein 1, 3584 CC Utrecht, The Netherlands.

Experimental Methods

Substrate preparation: Fused silica wafers with a thickness of 500 μm were diced into small chips. These were then cleaned by a three step process in an ultrasonic bath with acetone, isopropanol and ultrapure water. An oxygen plasma treatment (400 W, 2 min) was conducted days before the printing experiments. Molybdenum omniprobe half-grids (Pelco® Lift-Out TEM-Grids, TedPella Inc.) were used as a support for TEM analysis. The posts of the grids were cut/polished in a broad ion beam tool (IM4000, Hitachi) to ensure flat surfaces for printing without overhangs at the edge. They were then cleaned in an ultrasonic bath with acetone and visually inspected in an optical microscope.

Ink preparation: Printing inks were prepared using the recipe for colloidal gold nanocrystals of Zheng *et al.*[1] Briefly, solution A containing chloro(triphenyl phosphine) gold(I) (130 mg) in a mixture of toluene (25 mL) and dodecanethiol (500 μL), and solution B containing *tert*-butylamine borane (216 mg) in toluene (15 mL) were heated to 100°C under air. While at this temperature, solution B was added to solution A. After 45 min, the reaction mixture was allowed to cool down to room temperature. The gold nanocrystals produced were then washed by precipitation with ethanol and centrifugation, after which they were redispersed in hexane. This procedure yielded nanocrystals with a diameter of 4.5 ± 0.3 nm (mean ± standard deviation, from manual analysis in the software imageJ) in a dispersion with optical density at the first extinction peak of OD = 90 over 1 cm path length. Other sizes of nanocrystals could be obtained by reducing the amount of tert-butylamine borane and/or dodecanethiol used in the synthesis (see Figure S1).

The nanocrystals with an average diameter of 4.5 nm were used for the printing experiments presented in the main text. The native dodecanethiol ligands were first exchanged to octanethiol. To this end, the nanocrystal dispersion (500 μL) was mixed with hexane (4 mL) and octanethiol (500 μL) and heated to 50°C under air for 1 h. The nanocrystals were then precipitated with a methanol/ethanol mixture, centrifuged, and redispersed in hexane. The ligand-exchanged nanocrystal dispersion in hexane was then mixed with pure tetradecane in 1:2 (v/v) ratio. The mixture was left overnight in a fume hood to allow all hexane to evaporate. The resulting ink of gold nanocrystals dispersed in tetradecane was used for the printing experiments.

Printing nozzle fabrication: Nozzles with outer diameters of 1000-1200 nm were fabricated by pulling borosilicate glass capillaries (TW100-4, WorldPrecision Instruments) in a two-pull recipe using a Sutter Instruments P-97 pipette puller. To electrically contact the ink, they were then coated (e-beam evaporation, Plassys MEB550S) with a fine titanium adhesion layer and a gold layer with thicknesses of 5 and 50 nm, respectively.

EHD printing experiments: The nanowalls were fabricated on a 3-axis piezo-stage (MadCityLabs Nano-LP300), ensuring accurate and repeatable positioning. The growth rate of the nanowalls was observed using an objective (50×, NA 0.42, Edmund Optics Plan Apo ULWD) mounted at a 45° angle (see also Figure 1 in main text) The pipette was first brought to a relatively close distance to the substrate (~20 μm). Then the ink was pipetted into the capillary from the back and carefully pushed to the nozzle tip using a syringe pump. Next, the syringe was removed and the nozzle was positioned at the printing working distance of about 5–10 μm. The printing signal applied was a symmetric bipolar square wave with peak voltrage of 180 to 300 V and a frequency of 200 Hz–1 kHz. The printing velocity was in the range of 4 to 8 μm/s. The

growing nanowall was moved away from the nozzle to maintain a constant working distance. Tilt compensation ensured a constant working distance for the full length of lateral stage movement, which was essential for the printing onto the up-right posts of a TEM support grid. The silica chips were placed on a grounded indium tin oxide coated glass plate.

Thermal annealing: The printed structures were thermally annealed in a rapid thermal annealing system under atmospheric pressure (Annealsys AS150) and reducing conditions (50 sccm Ar/H_2 (5 vol% H_2)). The samples were heated to 400°C by a three-ramp program, first 10°C/s, then 2°C/s and for the last 10°C by 1°C/s (to prevent temperature overshoot), annealed for 20 min, and then cooled down to room temperature supported by a 200 sccm Ar purging gas flow. A 30-s argon sputtering step (Oxford NPG80, 140 W, 30 mTorr) was carried out to reduce the base width of the nanowalls prior to the annealing. This directional ion-milling removes 5-10 nm (1-2 monolayers of gold nanoparticles) of material from the top of the nanowalls, the extended nanoparticle base and the substrate, while not affecting the side walls. Figure S2a shows the extended base of an as-printed nanowall, i.e. before sputtering and annealing.

Transmission electron microscopy: Nanoparticle analysis was performed using a transmission electron microscope (JEOL JEM-1400 Plus) in bright-field mode (BF-TEM), operated at 120kV. The TEM support grids with printed and annealed nanowalls were analysed using a transmission electron microscope (Talos F200X, Thermofisher Scientific (formerly FEI)) in scanning mode (STEM), operated at 200kV. The bright-field STEM, low-angle annular and high-angle annular STEM detectors were used to analyse the microstructure. Elemental content analyses of the printed walls were performed using the energy dispersive X-ray (EDX) spectroscopy mode in STEM.

Grain size analysis: The average grain size was evaluated from STEM micrographs measured using the Heyn line intercept method.[2, 3] Nine images were analysed drawing nine lines each in random directions, with each line containing about ten grains. Each image was taken from a different nanowall. The nanowalls were printed onto two different samples, which were annealed separately.

Pad fabrication: Pads for 4-point probe measurements and contacts to the nanowalls were deposited by ion-beam induced deposition (IBID) of platinum from a trimethyl(methylcyclopentadienyl)platinum precursor at 30 kV in a Thermofisher Scientific Helios NanoLab 450 machine. Ion-beam currents of 2500 pA and 80 pA were used for the deposition of the pads and contacts, respectively. A 2-nm-thick Pt layer was deposited by a DC sputter tool for SEM samples (Q150T, Quorum Technologies) before the IBID step to reduce charging effects. The contribution to the conductance for the 4-point probe measurements was assessed by measuring the same Pt layer without the nanowall connection, see Figure S7. The resistances for comparable pad separation were four orders of magnitude higher than the ones of the measured nanowalls.

Electrical measurements: Electrical resistance of single gold nanowalls was measured by a Keithley 4200 source meter unit in a 4-point probe configuration (see Figure 4a in main text). This is necessary because of the relatively high contact resistance between the tungsten probe needles (7 μm tip radius) and the ion-beam deposited contact pads and in the narrow ion-beam deposited nanowall contacts. A 2-way current sweep was applied up to 1 mA. Up to 1 mA, corresponding to a current density range from 6 mA/$(\mu m)^2$ to 25 mA/$(\mu m)^2$ for the largest and smallest cross-sectional area, respectively, a resistance increase due to Joule heating of far less than 1% was observed. For current densities close to 100 mA/$(\mu m)^2$, the resistance

increase was measured to be about 10%. All measurements were taken in quiet mode with a sweep delay time of 0.26 ms. For the measurements of the sputtered 2 nm platinum films the maximally applied current was gradually reduced in order to stay within the voltage compliance of 2 V.

Geometrical characterization: The geometry and morphology of the printed and thermally annealed grids were analyzed by SEM (Zeiss ULTRA plus) and AFM imaging (Bruker Dimension FastScan). AFM scans were performed in tapping mode using a Bruker NCHV-A tip with 8 nm nominal tip radius. 3 scans, one in the center and one at each end, were made on each nanowall and 3 profiles were extracted from each scan. Out of the total number of 9 AFM profiles per nanowall the average maximum height was extracted. The error of the measurement is given as ±1 standard deviation. On average the standard deviation is 3% of the measured value. The length and width of the nanowalls were measured by SEM. The measured length was compared to the contact separation specified for the IBID process recipe and no measurable difference could be found. Width measurements were performed with placing three guidelines for the assumed width, an upper estimate and a lower estimate. Good-quality SEM pictures with high resolution were needed to ensure an accurate measurement. The cross-section was finally calculated assuming a rectangular profile to be on the conservative side.

ESI References

1.   N. Zheng, J. Fan and G. D. Stucky, *J Am Chem Soc*, 2006, **128**, 6550-6551.
2.   E. Heyn, *Metallographist*, 1903, **5**, 37-64.
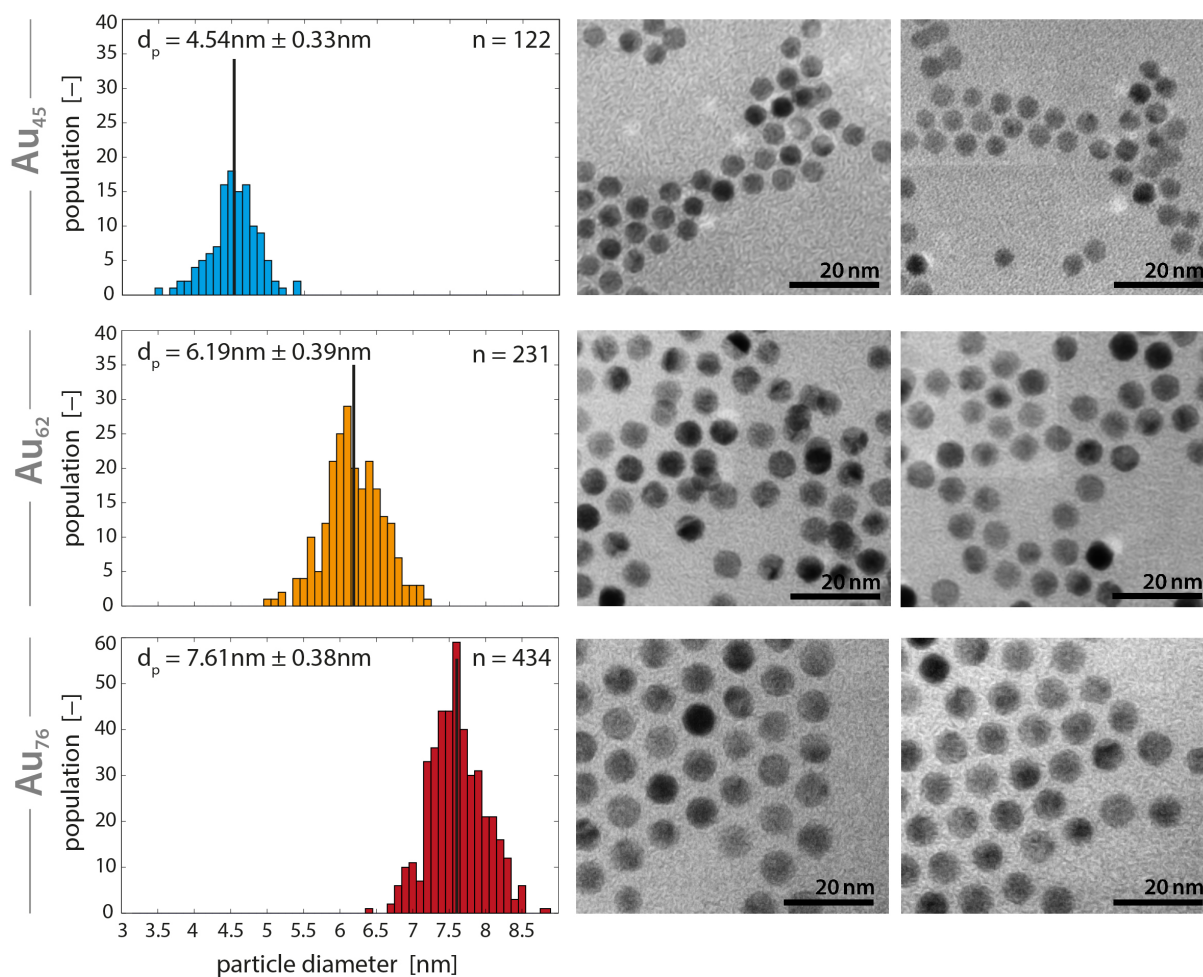3.   ASTM E112-12, 2012, DOI: https://doi.org/10.1520/E0112-12.

Supplementary Figures

Figure S1 - Gold nanoparticle size distributions of the inks Au$_{45}$, Au$_{62}$ and Au$_{76}$. Two representative BF-TEM micrographs are shown for each ink. The mean particle diameter and the standard deviation are given in the upper left corner of the histograms.
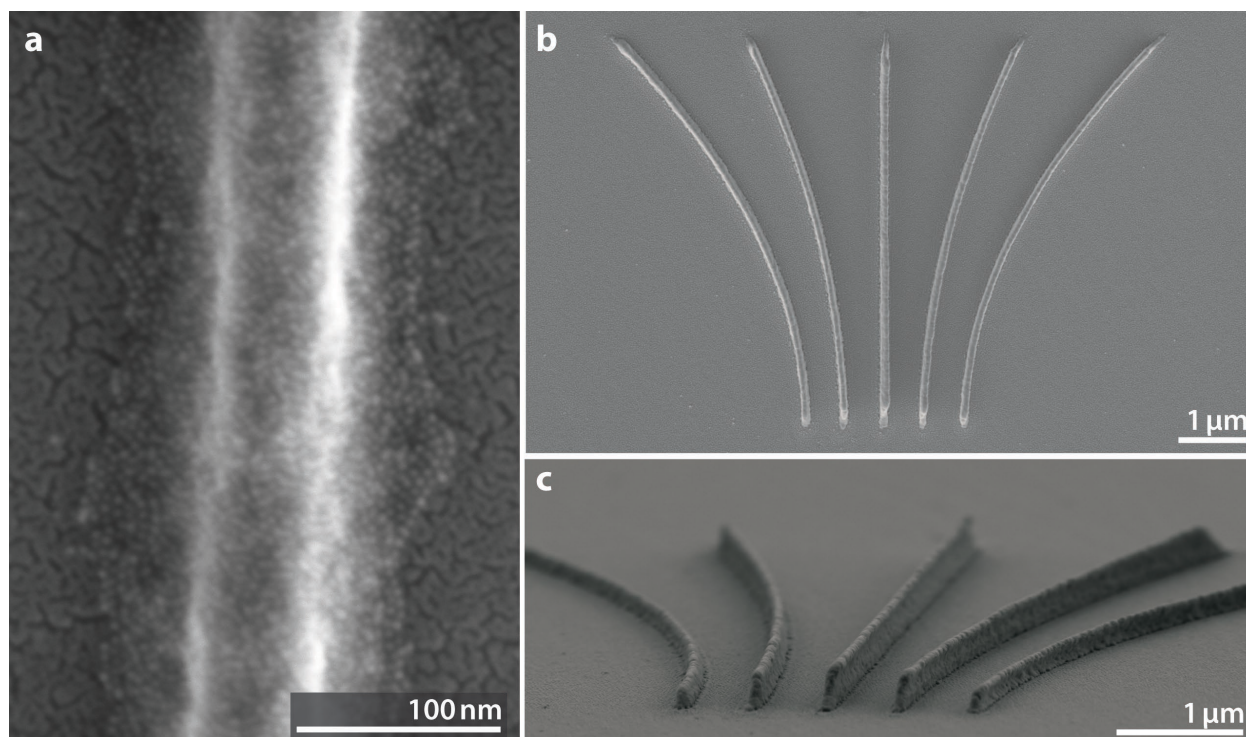
Figure S2 – 3D printing capabilities of EHD nanodripping. The high-resolution top view SEM **a** shows an as-printed gold nanoparticle assembly. The protruding nanowall has a width of 70 nm. Including the 1-2 monolayer thick foundation, the total width is about 140 nm. The SEM micrographs of annealed structures in **b** and **c** present the same set of curved nanowalls, each about 100 nm wide, imaged from the top and from the side at 75° tilt, respectively. The smallest pitch between the converging nanowalls, seen in the foreground of picture **c**, is 500 nm. The stage translation speed was 4 µm/s, the number of layers range from 12 to 20 for the outer walls and central wall, respectively. The assembly was deposited layer-by-layer to avoid large height differences during build-up.
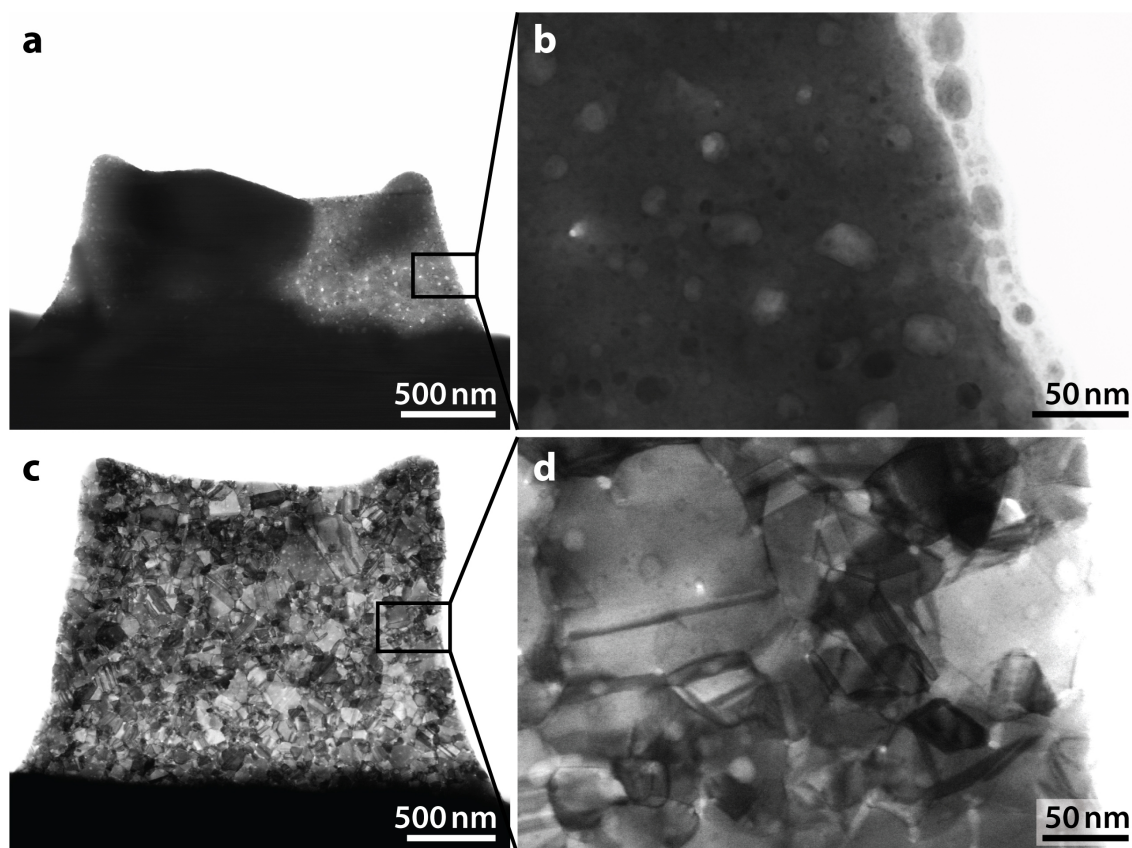
Figure S3 – BF-STEM images of two gold nanowalls annealed at different temperatures. The wall in **a**, annealed at a lower temperature of 280°C, is still partly covered with ligand residues. The magnified image **b** contains some clusters larger than the printed nanoparticles. The wall in **c**, annealed at 400°C, presents a dense polycrystalline structure. Image **d** shows a zoomed-in view of the right end of the nanowall.
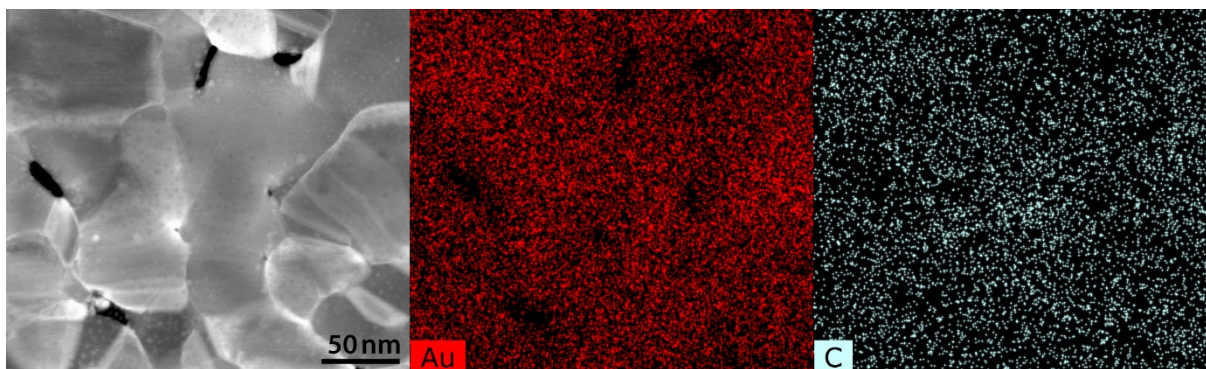
Figure S4 - HAADF-TEM micrograph with the EDX counts for gold and carbon. Dark spots in a dark field image indicate a region where fewer electrons are scattered towards the detector. These regions show a lower gold and carbon count.
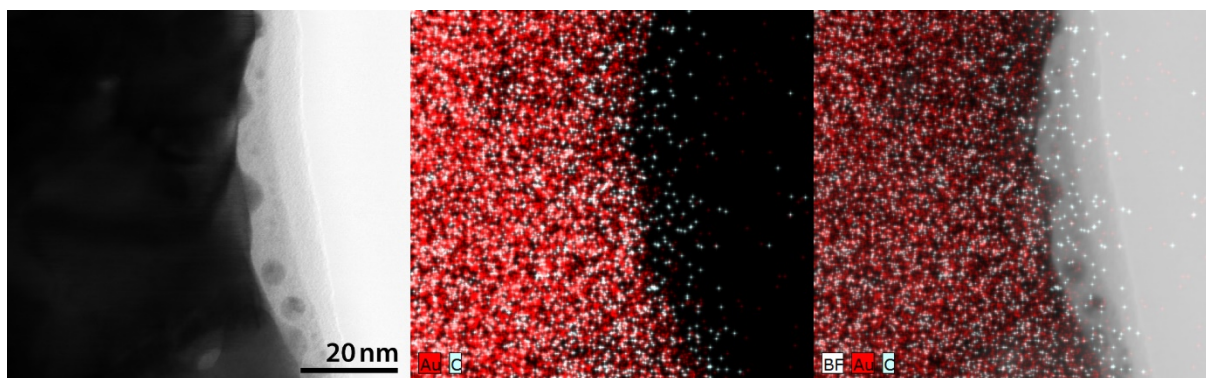

Figure S5 - BF-TEM image from the right end of a gold nanowall. The EDX signal indicates a thin layer of carbon surrounding the gold.
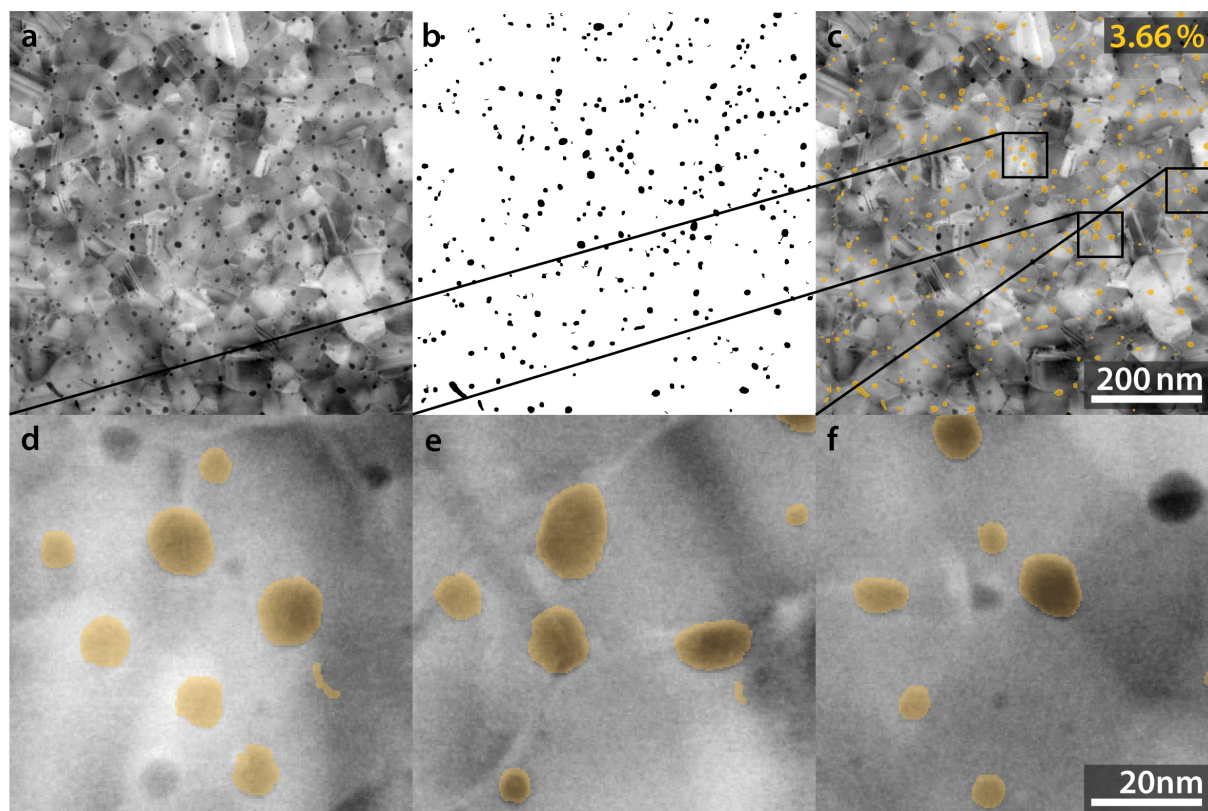
Figure S6 - Aerial inclusion fraction evaluation algorithm. **(a)** HAADF-STEM micrograph **(b)** Extracted areas **(c)** Overlay of **a** and **b (d,e,f)** Magnified regions of micrograph **c** with reduced opacity of the extracted areas, showing the slightly overestimated inclusion area.
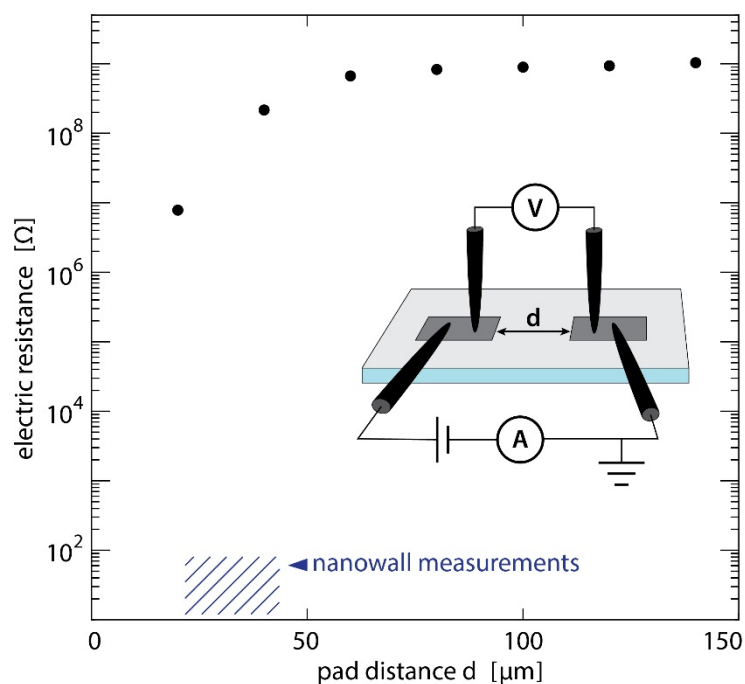
Figure S7 - Resistance measurements of the sputtered 2-nm-thick platinum film. 40 μm wide and 80 μm long pads were deposited by ion-beam induced deposition at conditions identical to the pads used for the nanowall measurements and placed at varying distances from each other. The pad distances and resistance measurement range is indicated as the blue hatched region, the 4-point probe setup is shown in the inserted schematic.
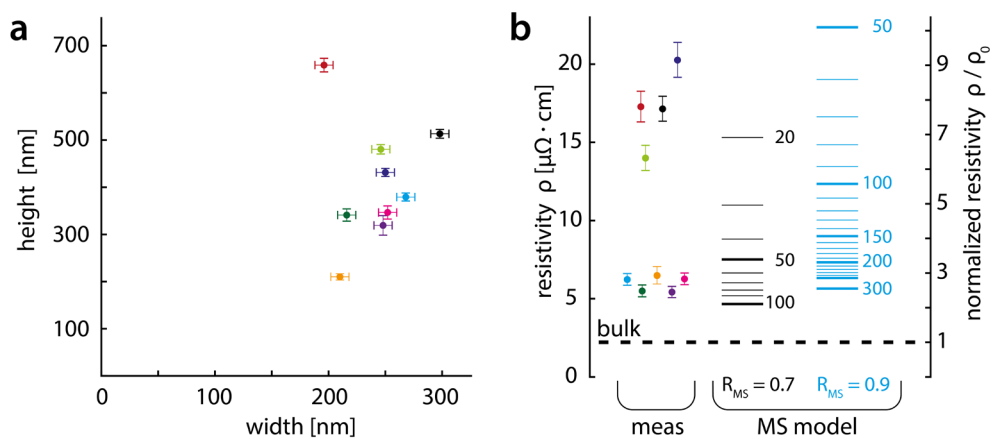

Figure S8 - **(a)** AFM height and SEM width measurements for the electrically measured gold walls. The assumed errors are described in the methods section. **(b)** On the left side the calculated resistivities based on equation (2) are shown with the same color-coding used in **a**. On the right side the values predicted by the grain-boundary-scattering model of Mayadas and Shatzkes are shown for a selection of grain sizes matching the resistivities measured. The black and blue dashes show the values for an electron reflectivity parameter of 0.7 and 0.9, respectively, while the numbers to the right of the dashes stand for the average grain size in nm used for the calculation.